RSC Advances

PAPER

View Article Online
View Journal | View Issue

Cite this: *RSC Adv.*, 2022, **12**, 2083

Synthesis of indeno-[1,2-*b*]-quinoline-9,11(6*H*,10*H*)-dione and 7,7-dimethyl-10-aryl-7,8-dihydro-5*H*-indeno[1,2-*b*]quinoline-9,11(6*H*,10*H*)-dione derivatives in presence of heterogeneous Cu/zeolite-Y as a catalyst†

Shankar D. Dhengale,[ab] Chandrashekhar V. Rode,[b] Govind B. Kolekar[c] and Prashant V. Anbhule *[a]

Received 3rd September 2021
Accepted 30th November 2021

DOI: 10.1039/d1ra06637d

rsc.li/rsc-advances

A simple method for the synthesis of indeno-[1,2-*b*]-quinoline-9,11-(6*H*,10*H*)-dione derivatives and 7,7-dimethyl-10-aryl-7,8-dihydro-5*H*-indeno[1,2-*b*]quinoline-9,11(6*H*,10*H*)-diones through the reaction of aromatic aldehydes, indan-1,3-dione, dimedone, and *p*-toluidine/ammonium acetate in the presence of heterogeneous CuO supported on a zeolite-Y catalyst has been investigated in ethanol under reflux conditions. By this method, the reaction time has been reduced, giving an excellent yield of the product. The catalyst was prepared by a hydrothermal method followed by a wet impregnation method. The catalyst had shown Brønsted acid sites and Lewis acid sites. The used catalyst could be actively recycled with a marginal decrease in yield up to five recycles. The prepared catalyst was characterized by FT-IR, pyridine FT-IR, XRD, SEM, EDS, XPS, TEM, and BET surface area analysis. The synthesized compounds were characterized by FT-IR, ^{1}H NMR, ^{13}C NMR and GC-MS spectroscopy.

1. Introduction

Nowadays, microporous and mesoporous materials with ordered porous structures are used as hosts to encapsulate metal particles of particular interest in catalysis because the framework stabilization can hinder the aggregation of transition metals and the pore size restraint could limit the development of clusters even at high temperatures.[1,2] Among microporous materials, zeolites have been the focus of more research work in the last few years, among the diverse types of hosts where semiconductor nanoparticles have been prepared.[3] Variety in pore size, shape, topology, and framework composition provides zeolites with a rich series of interesting properties and industrial applications, such as catalysts, ion exchangers, and adsorbents.[4]

The addition of Al to mesoporous MCM-41 increased the maximum adsorption capacity. Although zeolite NaX, which had a higher Al content than NaY, had a lower adsorption capacity, namely, 120 mg g^{-1}-adsorbent.[5] A Faujasite structure containing periodic supercages has been observed in zeolites X and Y.

The acidity and the activity of an aluminosilicate zeolite are determined by the aluminum content and the location of the Al in the zeolite crystal. The location of the Al is the fundamental tool needed for the zeolite activity. Additionally, an external surface of zeolite particles plays an important role in a lot of catalytic chemistry as large reactant molecules react primarily at the pore opening of the zeolite, such as in fluid catalytic cracking, as they cannot penetrate the smaller channels. Pore opening catalysis has been designed to provide experimental selectivity in selective isomerization, transalkylation, and hydrocarbon cracking.[6]

The commercial synthesis of Y zeolite was first declared by Breck[7] in 1964 following the first industrial manufacturing of A and X types by Milton.[8,9] Zeolite NaY emerged to be topologically comparable with the type X aluminosilicate framework. The most common way to make zeolite-Y is through hydrothermal synthesis. It is a natural process that efficiently creates crystalline silica and zeolites, among other minerals.[10] Zeolites are the cubic unit cell type of aluminosilicates which contain tetrahedral structures of SiO_4 and AlO_4. Zeolites with Si/Al values lower and higher than this critical point characterize X and Y compositions, respectively. Because of the instability of Al-rich samples in acids or water at elevated temperatures, Rüscher *et al.*[11] proposed a new definition based on the typical chemical

[a]*Medicinal Chemistry Research Laboratory, Department of Chemistry, Shivaji University, Kolhapur-416004, India. E-mail: pvanbhule@gmail.com*

[b]*Chemical Engineering and Process Development Division, CSIR-National Chemical Laboratory, Dr Homi Bhabha Road, Pune-411008, India*

[c]*Fluorescence Spectroscopy Research Laboratory, Department of Chemistry, Shivaji University, Kolhapur-416004, MS, India*

† Electronic supplementary information (ESI) available. See DOI: 10.1039/d1ra06637d

behavior of the samples under dealumination by steam treatment.[12] Faujasite zeolites are classified on the basic of silicon to aluminum ratio (Si/Al), so zeolite-X has an Si/Al ratio between 1 and 1.5 and zeolite-Y has an Si/Al ratio over 1.5.[13,14] Zeolites have three-dimensional structures with precise micropores or mesopores. The porous structure of a zeolite provides a large surface area that is suitable for the absorption ability of zeolitic materials and ensures their efficacy as an adsorbent in a variety of applications.[15]

At present, multi-component reactions (MCRs) occupy an outstanding position in organic and medicinal chemistry for their high degree of atom economy and applications in combinatorial chemistry due to their capability of preparing target molecules with atomic economy and high efficiency by the reaction of three or more starting materials together in a single step.[16,17] MCR has attracted increasing attention as one of the most powerful emerging synthetic tools for the construction of molecular diversity, complexity, and forming several bonds in a single operation. MCRs are usually associated with several advantages, such as the green process of bond-forming, shorter reaction times, operational simplicity, convergence, avoidance of time-consuming processes, energy and raw material saving, high bond-forming efficiency, minimal waste generation, reduction in the number of work-ups, as well as having no need for complicated purification processes.[18] MCRs have intrinsic advantages over two-component reactions: the simplicity of a one-pot procedure, possible structural variations, complicated synthesis, and a large number of accessible compounds.[19]

Nevertheless, continued efforts are being made to explore new MCRs for developing popular organic reactions.[20–24] Preferably, all reaction equilibria in the complex MCR mixture should be reversible, and the last, the product-designing reaction step, must be irreversible, thus providing the driving force to shift all intermediates and starting materials towards a single final product.[25]

A quinoline skeleton is present in a large number of biologically active compounds and possesses a broad spectrum of biological activities. Quinoline derivatives undergo hierarchical self-assembly into a variety of nanostructures and mesostructures with enhanced electronic and photonic functions as well as medicinal applications.[26]

Indenoquinoline derivatives showed a wide range of biological activities such as 5-HT-receptor binding activity,[27] anti-inflammatory activity and they also act as anti-tumor agents,[28] inhibitors for steroid reductase,[29] acetylcholinesterase inhibitors,[30] show antimycobacterial[31] and antiproliferative activities[32] and act as antimalarials.[33] Also, these compounds serve as the building blocks of many natural-chromophore DNA intercalators such as TAS 103,[34] DACA,[35,36] and NSC 314622,[37] which are currently being used as anticancer drugs. For this reason, much attention has been directed toward the synthesis of indenoquinoline derivatives *via* multi-component reactions. Shirini *et al.* newly described the synthesis of dihydro-5*H*-indeno[1,2-*b*]quinolines and showed that these compounds with stabilized zwitterionic resonance structures showed feasible application as new pH indicators. These chemosensors have a large wavelength shift (100 nm) and revealed excellent sensitivity in the pH range from 9.2 to 12.[38]

Many researchers have explored the preparation of copper surrounded by mineral networks, such as zeolite[39] and ZSM-5.[40] Zeolites acidic sites applied for copper grafting sites have microporous and crystalline aluminosilicates; they behave as an appropriate support, allowing the high dispersion of copper ions. In this Cu/zeolite-Y system, the copper oxidation states were explored by intense experimental characterization to understand the structure of the active site.[41–44] A high dispersion of copper ions is extensively engaged in catalysis. Their catalytic activity is due to the oxidation state, which may change easily under different environments and can be deduced from the relative stability of Cu(II) and Cu(I) oxidation states, which depends strongly on the nature of the counter-ion.[45,46] Several new methodologies have previously been reported for the synthesis of indenoquinoline derivatives *via* multi-component reactions in the presence of various catalysts, such as AcOH,[47], [bmim$^+$][BF4$^-$],[48] $H_{14}NaP_5W_{30}O_{110}$,[49] In(OTf)$_3$,[50] melamine trisulfonic acid (MTSA),[38] TiO_2 nanoparticles,[51] *p*-toluenesulphonic acid[18,25] tribromomelamine (TBM), SA, and $ZrOCl_2$.[52] These methods have their own merits and shortcomings. In this work, we report the preparation of a zeolite-Y supported copper catalyst using a two-step procedure: preparation of the zeolite-Y support using a hydrothermal method and copper(II) ions being introduced by using a wet impregnation method and drying followed by calcination at an optimum temperature.

2. Experimental

2.1 Preparation of zeolite-Y by hydrothermal process

2.1.1 (Composition – 4.62 Na_2O: Al_2O_3:10 SiO_2:180H_2O)

2.1.1.1 Part-I (seed gel). 1.2 g of sodium hydroxide (NaOH) was dissolved in 6 mL of water and kept under stirring (10 minutes). Into this solution 2 mL of sodium aluminate ($NaAlO_2$) was added and stirred until it was dissolved. Then 6.81 g of sodium silicate (Na_2SiO_3) solution was added and kept under further stirring for at least 10 min. After stirring, the solution was kept for aging in a closed bottle for one day.

2.1.1.2 Part-II (feedstock gel). 0.042 g of NaOH was added to 39 mL of water. 3.92 g of sodium aluminate ($NaAlO_2$) was

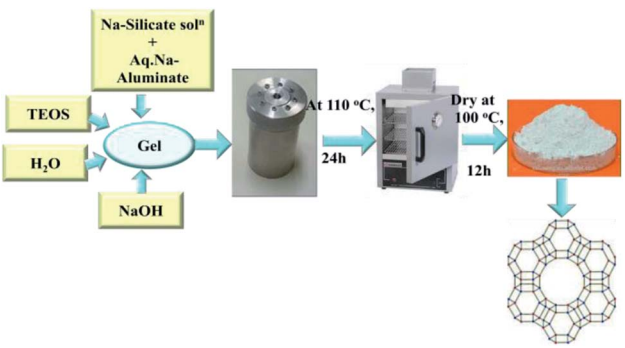

Scheme 1 Preparation of zeolite-Y.

Table 1 Preparation of various catalysts by a wet impregnation method

Entry	Catalyst	Precursor weight; g	Support weight; g	Solvent; mL	Calcination conditions		Activation conditions	
					Temp; °C	Time; h	Temp; °C	Time; h
1	Zn/Al_2O_3	$Zn(NO_3)_2 \cdot 6H_2O$; 0.4549	Al_2O_3; 0.9	Water; 10	300	3	450	2
2	Cu/Al_2O_3	$Cu(NO_3)_2 \cdot 3H_2O$; 0.380	Al_2O_3; 0.9	Water; 10	400	4	450	2
3	Co/Al_2O_3	$Co(NO_3)_2 \cdot 6H_2O$; 0.4938	Al_2O_3; 0.9	Water; 10	300	3	—	—
4	Zn/MCM-41	$Zn(NO_3)_2 \cdot 6H_2O$; 0.4549	MCM-41; 0.9	Water; 10	300	3	—	—
5	Cu/MCM-41	$Cu(NO_3)_2 \cdot 3H_2O$; 0.380	MCM-41; 0.9	Water; 10	400	4	—	—
6	Co/MCM-41	$Co(NO_3)_2 \cdot 6H_2O$; 0.4938	MCM-41; 0.9	Water; 10	300	3	—	—
7	Zn/zeolite-Y	$Zn(NO_3)_2 \cdot 6H_2O$; 0.4549	Zeolite-Y; 0.9	Water; 10	300	3	—	—
8	Cu/zeolite-Y	$Cu(NO_3)_2 \cdot 3H_2O$; 0.380	Zeolite-Y; 0.9	Water; 10	400	4	—	—
9	Co/Zeolite-Y	$Co(NO_3)_2 \cdot 6H_2O$; 0.4938	Zeolite-Y; 0.9	Water; 10	300	3	—	—
10	Cu/SiO_2	$Cu(NO_3)_2 \cdot 3H_2O$; 0.380	SiO_2; 0.9	Water; 10	400	4	—	—

dissolved in this solution and mixed until it was dissolved. Into this solution 42.72 g of sodium silicate (Na_2SiO_3) solution was added and stirred vigorously with a high-shear turbine mixer.

2.1.1.3 Part-III (overall gel). Feedstock gel was added slowly to 4.95 g of seed gel and stirred with a high-shear turbine mixer for 30 minutes.

The whole solution was kept for crystallization in a polypropylene bottle at room temperature for 24 h by incubation, and then kept in an oven at 100 °C for 7 h. The product was recovered by filtration and washed with water up to pH less than 9. The recovered product was dried at 100 °C. See Scheme 1 for an overview of the process.

2.2 Wet impregnation method

Various catalysts which require compositions of Zn, Cu, and Co on different supports were prepared by a wet impregnation method. In this preparation method, an appropriate amount of precursor was dissolved in water or ethanol as solvent. Further solid support was added portion-wise to this solution with constant stirring for the next 12 h. The solvent was evaporated from the impregnated samples and dried at 110 °C for 12 h. The solvent was evaporated from the impregnated samples and they were dried at 110 °C for 12 h. The prepared catalysts were then calcined (Table 1 entries 1–10) and activated by an H_2 atmosphere (Table 1 entries 1 and 2).

3. Result and discussion

3.1 Characterization of catalyst

FT-IR peaks at 463, 505, 578, 717, 792, 1022, 1141, 1339, and 3452 cm^{-1} were found in commercial zeolite-Y. The prepared zeolite-Y showed peaks at 677, 752, 999, 1506, 1547, 1652, 1692, 1735, 2334, 2915, 2927, 3464, 3746, and 3866 cm^{-1} (ref. [53]) (Fig. 1). It has been reported that for BAS, the band at 1540–1550 cm^{-1} can be used for quantification of protonated pyridine, while the band at 1440–1450 cm^{-1} can be used for molecularly adsorbed pyridine for LAS and the peak at 1490 cm^{-1} peak contains contributions from both Brønsted and Lewis acidity.[54] Herein, the peak was shifted from 1490 cm^{-1} to 1651 cm^{-1} for zeolite-Y.

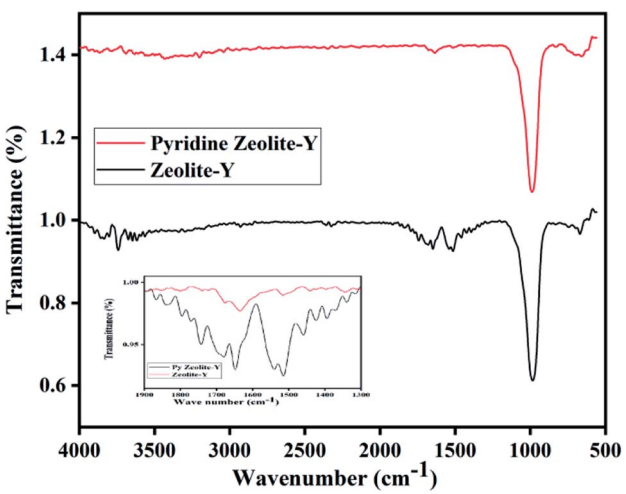

Fig. 1 IR spectra of zeolite-Y before pyridine adsorption and after pyridine adsorption.

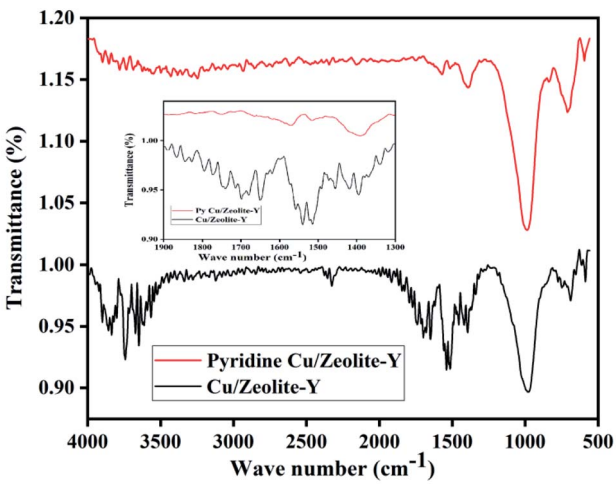

Fig. 2 IR spectra of Cu/zeolite-Y before pyridine adsorption and after pyridine adsorption.

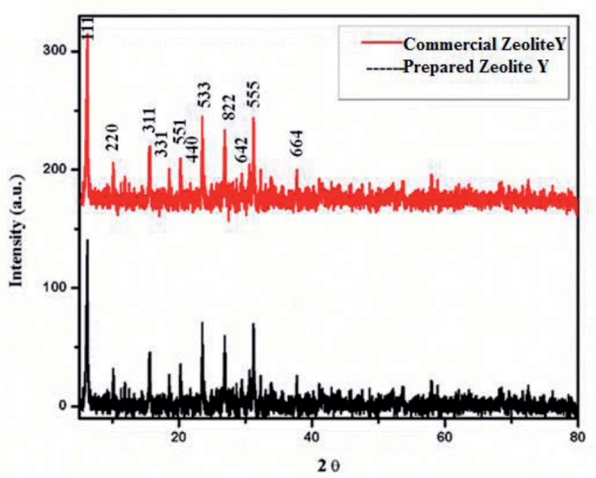

Fig. 3 X-ray diffraction patterns of commercial and prepared zeolites-Y.

Cu/zeolite-Y shows peaks at 589, 677, 752, 999, 1506, 1547, 1652, 1692, 1735, 2334, 2915, 2927, 3464, 3746, and 3866 cm^{-1} (ref. [55]) in the FT-IR. It has been observed that the FT-IR spectrum of zeolite-Y and Cu/zeolite-Y showed a broad peak at 999 cm^{-1} in zeolite-Y which was reduced when Cu metal was added to some sites. In Cu/zeolite-Y, the band at 1574 cm^{-1} was observed due to pyridine adsorption having both Brønsted and Lewis acid sites (Fig. 2).

The XRD pattern of zeolite-Y support showing 2θ values at: 6.22° (1 1 1), 9.97° (2 2 0), 11.85° (3 1 1), 15.61° (3 3 1), 18.65° (5 5 1), 20.24° (4 4 0), 23.56° (5 3 3), 27.18° (8 2 2), 27.74° (6 4 2), 29.76° (8 2 2), 30.64° (5 5 5), 32.22° (8 4 0), and 33.96° (664) corresponds to Si in its SiO_2 and Al in its Al_2O_3 forms (Fig. 3) (JCPDS: 43-0168).[56] 2θ values in our prepared zeolite-Y catalyst match exactly with the commercial zeolite-Y sample, which clearly confirms the successful preparation of the zeolite-Y catalyst. The commercial and prepared zeolite-Y were validated by XRD. Peaks at $2\theta = 48.5°$ (2 0 2), 51.3° (1 1 2), 53.4° (0 2 0), and 61.4° (1 1 3) were assigned to monoclinic end centred CuO phases [JCPDF File No. 801917] (Fig. 4). Only two CuO signature peaks at 35.48° and 38.92°, which were assigned to the (2 0 0) and (0 0 2) planes (JCPDS 80-1268), were observed for both CuO and zeolite systems, confirming the formation of CuO on zeolite.[57]

Determination of Cu/SiO_2 shows a strong and broad peak in the ranges of $2\theta = 5°$ and 15–35° due to amorphous silica with no diffraction peaks for Cu, probably because the amount of Cu within SiO_2 is too small. The diffraction peaks (2θ) at 43.34°, 50.47°, and 74.17° are attributed to the (1 1 1), (2 0 0), and (2 2 0) planes of Cu, respectively, which can be undoubtedly be indexed to cubic Cu (JCPDS No. 04-0836).[58] For Cu/MCM-41 the strong peaks (2θ) at 43.9°, and 45.5° are attributed to the (1 1 0), (2 0 0), and (2 2 0) planes.[59] For Cu/Al_2O_3 the diffraction peaks of the samples correspond to the characteristic face centered cubic (FCC) copper lines indexed as (1 1 1), (0 0 2) and (0 2 2) that were observed in these samples at diffraction angles of 43.2°, 50.3° and 73.9°, respectively (JCPDS No. 98-000-9057).[60] XRD patterns of calcined 10% Cu/zeolite-Y and 10% Cu/SiO_2 show that copper is present in CuO phases (2θ at 36° and 39°).

These peaks are related to CuO (JCPDS: 45-0937). In summary, from the XRD patterns, except for pure CuO and zeolite, no other phases or other impurities, such as Cu or Na, were detected. For all CuY samples (except 10 CuY), these results can be accredited to well-dispersed Cu species interacting with the zeolite framework and there was no new phase formation despite high-temperature treatment at 550 °C.[61] Although two weak XRD diffraction peaks of NaY zeolite correlated to (222) and (422) planes disappear in the patterns of HY and CuY. The disappearance of these peaks may be recognized as local defect sites and the hydrolysis of a small fraction of Al–O bonds during the sudden exposure of the calcined samples to air.[62] Besides the diffractogram of zeolite-Y, the diffraction pattern of 10% CuY also displays low-intensity peaks at

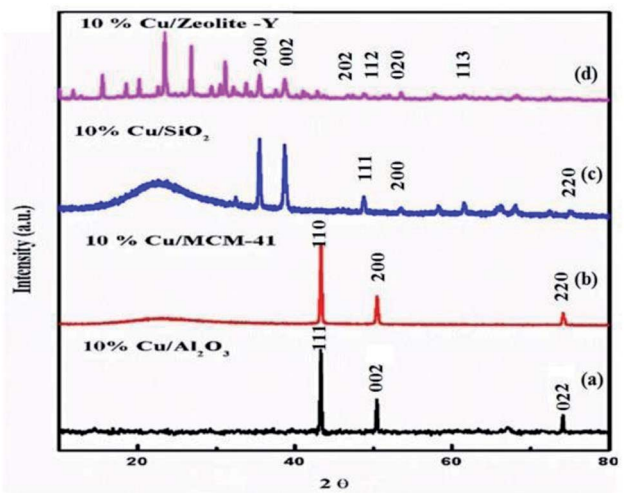

Fig. 4 X-ray diffraction study of Cu on different supports.

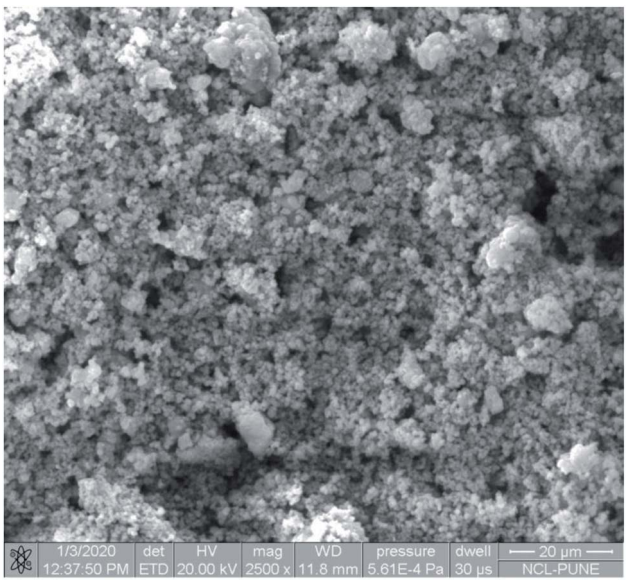

Fig. 5 SEM image of Cu/zeolite-Y.

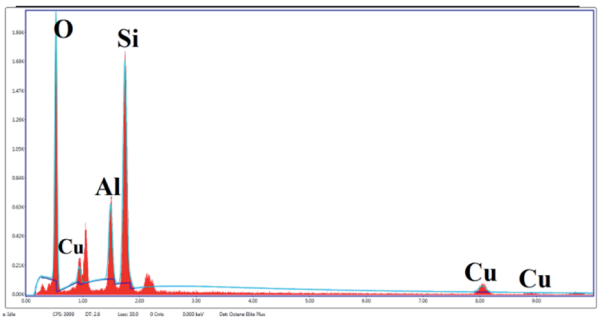

Fig. 6 EDS elemental analysis of Cu/zeolite-Y.

Table 2 EDS elemental analysis

Element	Weight%	Atomic%	Net int.	Error%
O K	48.95	64.85	629.46	7.89
Al K	10.55	8.28	268.40	6.73
Si K	31.73	23.95	811.90	5.18
Cu K	8.77	2.92	49.10	10.80

diffraction angles of 35.5° and 38.7° corresponding to [1, 1, −1] and [1, 1, 1] planes, respectively, of monoclinic CuO crystallite (JCPDF files 48-1548). These low-intensity peaks and their large FWHM suggest the presence of small copper oxide particles inside the pores of the zeolite. It was found that the intensity of all peaks decreased with metal loading, which occurred due to the absorption of X-rays by a layer of copper species.[63] Armengol *et al.* also detected a decrease in the intensity of the diffraction pattern of Y Faujasite as Na^+ ions exchange with Cu^{2+} ions[64] (Fig. 4). Hence, this Cu^{2+} ion may provide a Lewis acid site to the catalyst, which is useful for selective product formation.

The SEM image reveals that some particles are agglomerates. In addition, in SEM images of Cu/zeolite-Y it was also detected that copper nanoparticles are much smaller than zeolite-Y but have identical nanoparticle morphology to zeolite-Y (Fig. 5). The chemical purity of the samples was investigated by EDS (Fig. 6 and Table 2).

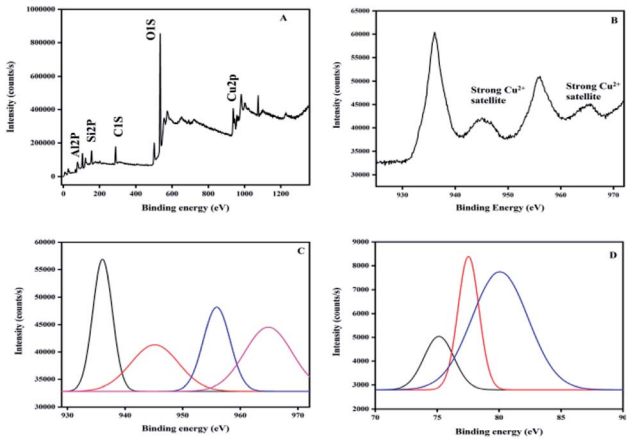

Fig. 7 XPS spectra of Cu/zeolite-Y: (A) survey, (B) Cu 2p, (C) Gaussian curves for Cu 2p, and (D) Gaussian curves for Al 2p.

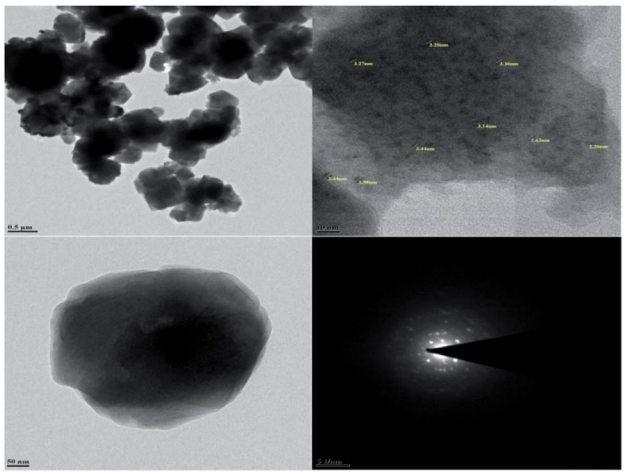

Fig. 8 TEM images of Cu/zeolite-Y.

The peaks of Si, Na, Al, and O signals were observed after calcination. The XRD patterns show that copper oxides exist in the zeolite. As per the EDS analysis, the mole ratios of copper to oxygen were 1 : 5, in good agreement with the XRD analysis (Fig. 6).

The XPS survey shows copper on the surface of the zeolite as well as the Na, Si, Al, and O of the structure of the zeolite, as shown in Fig. 7A.

The hybrid systems have no species contaminating them, but a very small amount of carbon (C 1s at 284.6 eV) used for calibration is detected. The O 1s core-level spectrum is given in Fig. 7A.

An analysis of the two Gaussian curves (I and II) was performed using curve-fitting. The peak located at 534 eV (I) is for the O^{2-} ion in CuO and the one at 536.8 eV (II) is for the oxygen adsorbed on the CuO surface. The peaks corresponding to Cu $2p_{3/2}$ and Cu $2p_{1/2}$ are observed at 936.18 eV and 956.01 eV, respectively. These values are in good agreement with the previously reported values of CuO.[65–67] On the high-binding-energy side, the Cu $2p_{3/2}$ peak is separated by about 9 eV from its strong satellite. A d^9 electron ground state configuration is

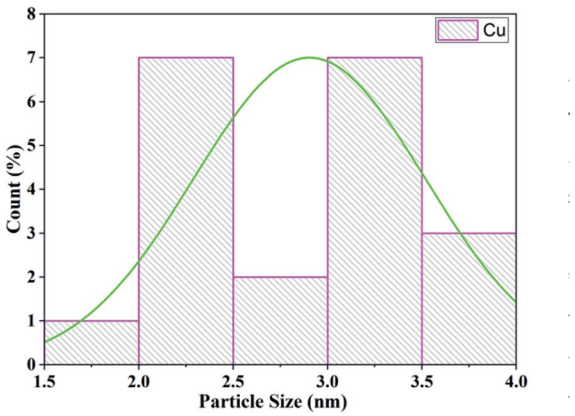

Fig. 9 Particle size distribution of Cu/zeolite-Y.

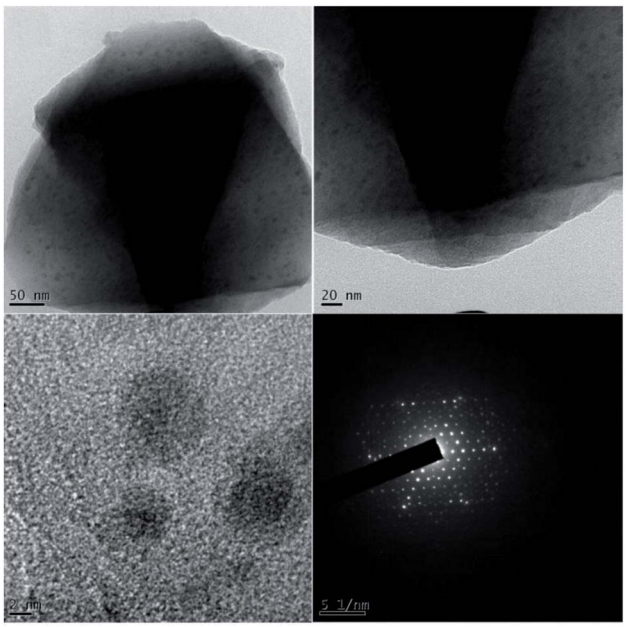

Fig. 10 TEM images of Zn/zeolite-Y.

characteristic of materials (*i.e.* CuO) that exhibit this property.[68] The core level Al 2p peak at 75 eV confirmed that Al is present as the Al_2O_3 form.[69] In conclusion, the XPS results demonstrate that the synthesized hybrid systems contain copper oxide, where copper is in an oxidation state of two. The zeolite-Y and copper oxide act as Brønsted acids as well as Lewis acids for the synthesis of indeno[1,2-*b*]quinoline-9,11(6*H*,10*H*)-dione derivatives.

Transmission electron microscopy (TEM) was used to investigate the size and morphology of the material. The distribution of copper oxide particles and the shape of zeolite-supported copper catalysts are shown in Fig. 8. There was well-dispersed copper oxide on the zeolite crystal. The average particle size of the impregnated copper was 2.90 nm. Copper nanoparticles of sizes of 5 to 2 nm with rather uniform spatial distribution were reported to predominate in the specimens (Fig. 9).[70]

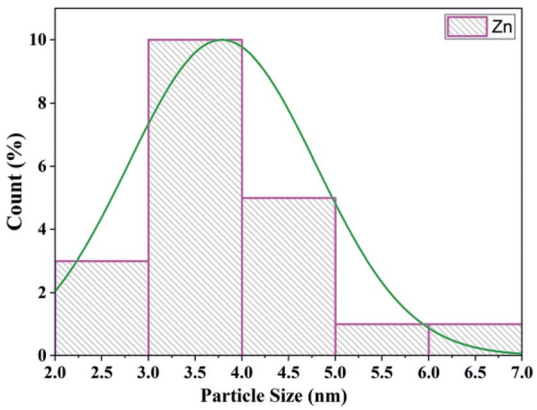

Fig. 11 Particle size distribution of Zn/zeolite-Y.

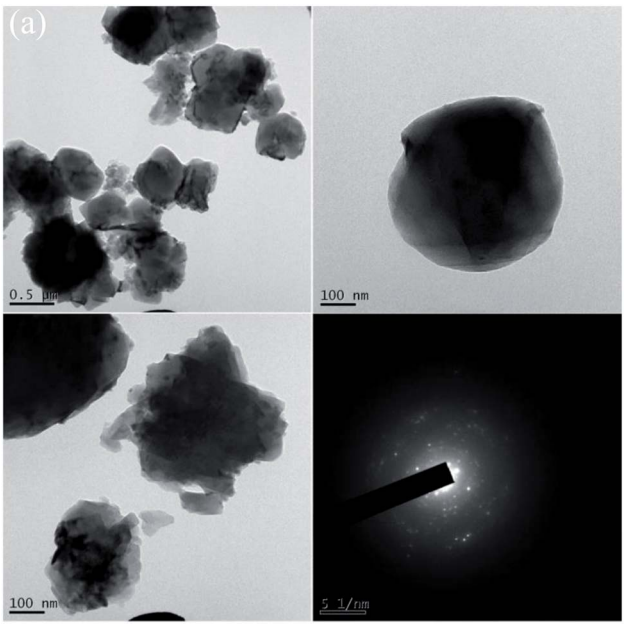

Fig. 12 TEM images of Co/zeolite-Y.

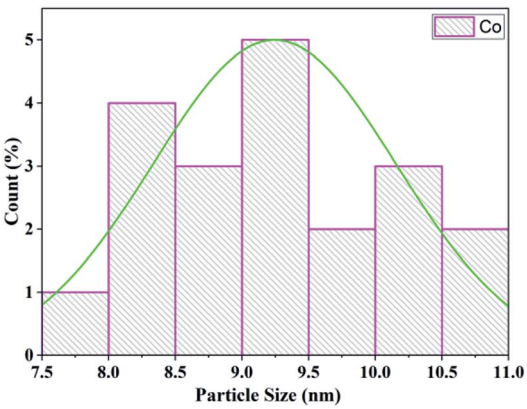

Fig. 13 Particle size distribution of Co/zeolite-Y.

The TEM analysis of Zn/zeolite explored the morphology and particle size. The distribution of zinc particles and the shape of zeolite-supported zinc catalysts are shown in Fig. 10. The

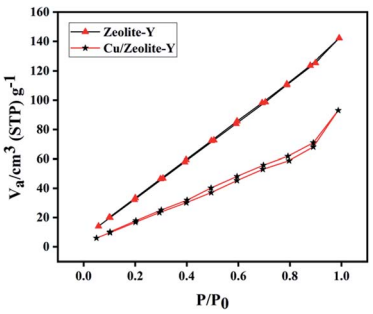

Fig. 14 N_2 adsorption–desorption isotherms of zeolite-Y and Cu/zeolite-Y catalysts.

Table 3 Optimization of reaction conditions for the synthesis of indeno-[1,2-*b*]-quinoline-9,11-(6*H*,10*H*)-dione derivatives

Entry	Catalyst	Amount (mg)	Solvent	Temperature (°C)	Time (min)	Yield (%)
1	Al_2O_3	10	EtOH	R.T.	180	—
2	Al_2O_3	10	EtOH	Reflux	180	Trace
3	SiO_2	10	EtOH	R.T.	180	—
4	SiO_2	10	EtOH	Reflux	180	—
5	MCM-41	10	EtOH	R.T.	180	—
6	MCM-41	10	EtOH	Reflux	180	—
7	Zeolite-Y	10	EtOH	R.T.	180	25
8	Zeolite-Y	10	EtOH	Reflux	180	39
9	CuO	10	EtOH	R.T.	180	30
10	CuO	10	EtOH	Reflux	180	55
11	Cu/SiO_2	10	EtOH	R.T.	180	30
12	Cu/SiO_2	10	EtOH	Reflux	180	55
13	Cu/Al_2O_3	10	EtOH	R.T.	180	33
14	Cu/Al_2O_3	10	EtOH	Reflux	180	38
15	Cu/MCM-41	10	EtOH	R.T.	180	36
16	Cu/MCM-41	10	EtOH	Reflux	180	42
17	Cu/zeolite-Y	10	EtOH	R.T.	180	60
18	**Cu/zeolite-Y**	**10**	**EtOH**	**Reflux**	**180**	**86**
19	Zn/Al_2O_3	10	EtOH	Reflux	180	27
20	Co/Al_2O_3	10	EtOH	Reflux	180	30
21	Zn/MCM-41	10	EtOH	Reflux	180	40
22	Co/MCM-41	10	EtOH	Reflux	180	43
23	Zn/zeolite-Y	10	EtOH	Reflux	180	38
24	Co/zeolite-Y	10	EtOH	Reflux	180	37
25	Cu/zeolite-Y	10	MeOH	R.T.	180	46
26	Cu/zeolite-Y	10	MeOH	Reflux	180	52
27	Cu/zeolite-Y	10	Acetonitrile	R.T.	180	38
28	Cu/zeolite-Y	10	Acetonitrile	Reflux	180	49
29	Cu/zeolite-Y	10	Toluene	R.T.	180	25
30	Cu/zeolite-Y	10	Toluene	Reflux	180	56
31	Cu/zeolite-Y	10	DCM	R.T.	180	—
32	Cu/zeolite-Y	10	DCM	Reflux	180	—
33	Cu/zeolite-Y	10	DMF	R.T.	180	—
34	Cu/zeolite-Y	10	DMSO	R.T.	180	—
35	Cu/zeolite-Y	10	Solvent free	100	180	—
36	**Cu/zeolite-Y**	**15**	**EtOH**	**Reflux**	**180**	**90**
37	Cu/zeolite-Y	20	EtOH	Reflux	180	91
38	Cu/zeolite-Y	25	EtOH	Reflux	180	93
39	Cu/zeolite-Y	30	EtOH	Reflux	180	93

average particle size of zinc impregnated on zeolite was 3.80 nm (Fig. 11) and for zeolite/zinc oxide, the mean grain size measured by the image program was estimated to be 4.3 nm.[71]

The morphology and particle size of the Co/zeolite catalyst was investigated from the TEM images. The particle size distribution of cobalt and the shape of the Co/zeolite-Y catalyst are shown in Fig. 12. The average particle size of the zeolite-Y supported cobalt catalyst was 9.25 nm (Fig. 13) which was determined from a histogram of the particle size distribution.

From the catalytic activity study, it was found that for synthesis of indeno-[1,2-*b*]-quinoline derivatives, selectivity was enhanced due to the Lewis acid sites as well as the Brønsted

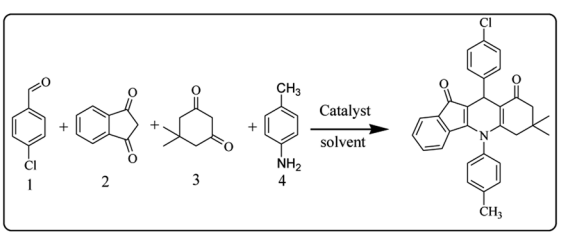

Scheme 2 Model reaction for the synthesis of indeno-[1,2-*b*]-quinoline-9,11-(6*H*,10*H*)-dione derivatives.

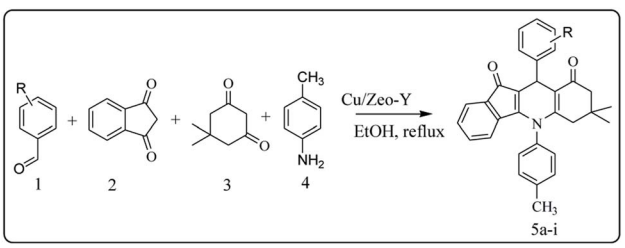

Scheme 3 Synthesis of indeno-[1,2-*b*]-quinoline-9,11-(6*H*,10*H*)-dione derivatives by using heterogeneous Cu/zeolite-Y as catalyst.

Table 4 Synthesis of indeno-[1,2-*b*]-quinoline-9,11-(6*H*,10*H*)-dione derivatives using a heterogeneous Cu/zeolite-Y catalyst[a,b]

Entry	Aldehydes	Aromatic amine	Product	Time in min	Yield (%)
5a			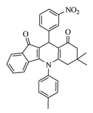	180	95
5b	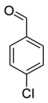		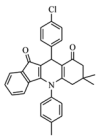	180	90
5c	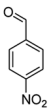		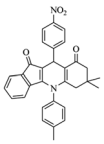	180	94
5d	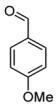		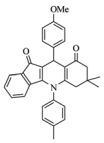	180	84
5e	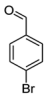		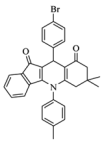	180	89
5f	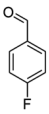		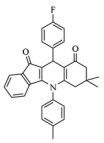	180	93
5g			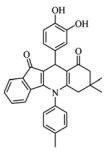	180	82
5h			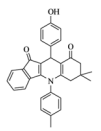	180	85
5i	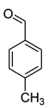		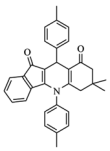	180	87

[a] Reaction conditions: substituted aromatic aldehydes (1 mmol), 1, 3-indandione, (1 mmol), dimedone (1 mmol), and *p*-toluidine (1 mmol), ethanol (5 mL) under reflux conditions in the presence of Cu/zeolite-Y (15 mg). [b] The yields refer to the isolated product.

acid sites supplied by Cu/zeolite-Y. This was supplemented by copper, zinc, and cobalt supported zeolite-Y catalysts for enhanced selectivity towards the product due to the copper particle size.

The BET (Brunauer–Emmett–Teller) surface areas of zeolite-Y and Cu/zeolite-Y were 178 $m^2\ g^{-1}$ and 96 $m^2\ g^{-1}$, respectively. Zeolite-Y and Cu/zeolite-Y have pore diameters and pore volumes of 1.816 nm and 1.801 nm, and 0.186 $cm^3\ g^{-1}$ and 0.129 $cm^3\ g^{-1}$, respectively. The results suggest partial blockage of the zeolite network by copper oxide species.[72] The N_2 adsorption–desorption isotherm of the Cu/zeolite-Y catalyst is shown in Fig. 14.

3.2 Optimization of reaction parameters

We have tested different supports like Al_2O_3, MCM-41, SiO_2, and zeolite-Y and it was observed that the zeolite-Y support forms the product (Table 3 entries 1–8). Also CuO used as the catalyst showed a yield (Table 3 entries 9 and 10). From these results, we have confidence that CuO shows activity for this synthesis. Hence supporting it with Cu/SiO_2, Cu/Al_2O_3, Cu/MCM-41, and Cu/zeolite-Y showed results (Table 3 entries 11–18). Cu/zeolite-Y shows an 86% yield of product (Table 3 entry 18). After that, the Zn and Co supported catalyst was tested for its activity (Table 3 entries 19–24). Then solvents like MeOH, acetonitrile, toluene, DCM, DMF, DMSO and solvent-free conditions were used for the reaction (Table 3 entries 25–35). After checking the catalytic activity of various catalysts, the Cu/zeolite-Y catalyst was found to be efficient for this reaction. Catalyst amounts from 10, 15, 20, 25, to 30 mg were checked for their activity, and about 15 mg of catalyst was sufficient for the transformation (Table 3 entries 18, 36–39). The model reaction (Scheme 2) afforded better yield in ethanol under reflux conditions. Both Lewis acid sites and Brønsted acid sites for the selective synthesis of indeno[1,2-*b*]-quinoline-9,11-(6*H*,10*H*)-dione derivatives were offered by the Cu/zeolite-Y catalyst apart from the Cu/SiO_2, Cu/Al_2O_3, and Cu/MCM-41 catalysts.

After optimization of the model reaction for the synthesis of indeno-[1,2-*b*]-quinoline-9,11-(6*H*,10*H*)-dione derivatives, we carried out a one-pot multicomponent reaction of aromatic aldehyde (1 mmol), 1,3-indandione, (1 mmol), dimedone (1 mmol), and *p*-toluidine (1 mmol) in ethanol as a solvent under reflux conditions (Scheme 3) with a heterogeneous catalyst Cu/zeolite-Y(0.015 g). We concentrated our attention on substrate diversity to confirm the generality of a protocol using substituted aromatic aldehydes and a screening test of various aldehydes was utilized. The electron-withdrawing *m*-nitrobenzaldehyde forms an excellent yield (95%) of the product (**5a**). Also, the electron-donating group *p*-chlorobenzaldehyde gives the corresponding product (**5b**) with a better yield of 90%. As summarized in Table 4, diverse functional groups of aromatic aldehydes (of electron-withdrawing or donating nature) react smoothly with each other to give a product with excellent yield (Table 4 entries 5a–5i).

From the above study, we concluded that substituted aldehydes proceeded to give the desired products with high yields.

For the synthesis of 7,7-dimethyl-10-aryl-7,8-dihydro-5*H*-indeno-[1,2-*b*]-quinoline-9,11(6*H*,10*H*)-diones derivatives using Cu/zeolite-Y as a heterogeneous catalyst, we carried out a one-pot multi-component reaction of aromatic aldehyde (1 mmol), 1,3-indandione, (1 mmol), dimedone (1 mmol), ammonium acetate (1.5 mmol) in ethanol (5 mL) as solvent (Scheme 4) and heterogeneous catalyst Cu/zeolite-Y. The current approach provides an excellent yield (82–96%) of the product (Table 5 entries 7a–h) in a quick reaction time due to its simple set-up, and there is no need for further product purification. The electron-withdrawing *m*-nitrobenzaldehyde gives an excellent yield of 94% (**7a**). Also, the electron-donating group *p*-chlorobenzaldehyde gives the

Table 5 Formation of 7,7-dimethyl-10-aryl-7,8-dihydro-5*H*-indeno-[1,2-*b*]-quinoline-9,11(6*H*,10*H*)-dione derivatives using a heterogeneous Cu/zeolite-Y catalyst[a,b]

Entry	Aromatic aldehydes	Product	Time in min	Yield (%)
7a	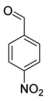	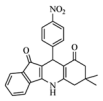	50	94
7b	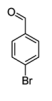	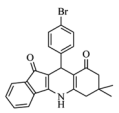	50	93
7c	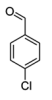	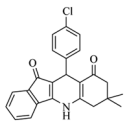	50	96
7d	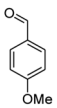	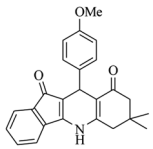	50	88
7e		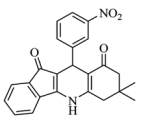	50	95
7f	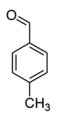	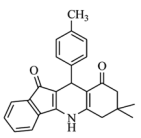	50	89
7g	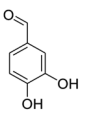	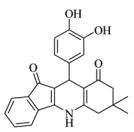	50	86
7h		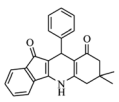	50	82

[a] Reaction conditions: substituted aromatic aldehydes (1 mmol), 1,3-indandione, (1 mmol), dimedone (1 mmol), and ammonium acetate (1.5 mmol), ethanol (5 mL) under reflux conditions in the presence of Cu/zeolite-Y (15 mg). [b] The yields refer to the isolated product.

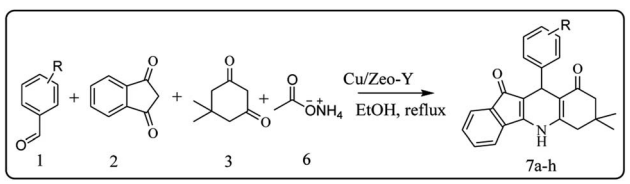

Scheme 4 Synthesis of 7,7-dimethyl-10-aryl-7,8-dihydro-5*H*-indeno-[1,2-*b*]-quinoline-9,11(6*H*,10*H*)-dione derivatives.

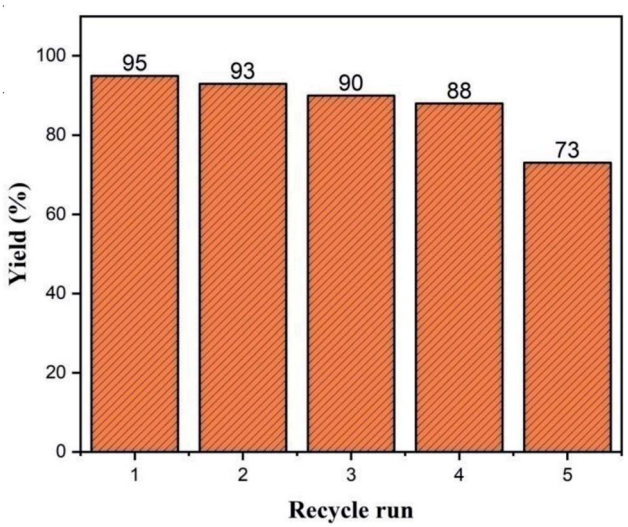

Fig. 15 Catalyst recycling experiment with Cu/zeolite-Y.

corresponding product (**7c**) with a better yield of 96%. This is summarized in Table 5.

3.3 Catalyst recycles

Even after five recycles under the optimum reaction conditions, the activity of Cu/zeolite-Y remained steady, as shown in Fig. 15. The catalyst was rinsed with ethyl acetate after each cycle, dried at 110 °C, calcined and reused.

4. Conclusions

In conclusion, pyridine FT-IR analysis has demonstrated that the Cu/zeolite-Y catalyst contains Brønsted and Lewis acid sites, while TEM images suggest that the particle size is optimal for the selective synthesis and high yields of indeno-[1,2-*b*]-quinoline-9,11-(6*H*,10*H*)-dione and 7,7-dimethyl-10-aryl-7,8-dihydro-5*H*-indeno-[1,2-*b*]-quinoline-9,11(6*H*,10*H*)-dione derivatives. This heterogeneous catalyst exhibits high activity, catalyst recovery, reusability, facile separation from products and a good to excellent yield of product in a short reaction time due to eliminating column chromatography, an easy workup and there being no need for further product purification.

Conflicts of interest

The authors announce no competing financial interest.

Acknowledgements

Shankar Dhengale acknowledges the Chhatrapati Shahu Maharaj Research, Training and Human Development Institute (SARTHI), Pune, MH, India, for the award of Chief Minister Special Research Fellowship.

References

1 Q. Tang, Q. Zhang, P. Wang, Y. Wang and H. Wan, *Chem. Mater.*, 2004, **16**, 1967–1976.
2 A. Seidel and B. Boddenberg, *J. Mater. Chem.*, 1999, **9**, 2495–2498.
3 M. R. Lukatskaya, A. S. Vyacheslavov, A. V. Lukashin, Y. D. Tretyakov, O. M. Zhigalina and A. A. Eliseev, *J. Magn. Magn. Mater.*, 2009, **321**, 3866–3869.
4 M. E. Davis, *Nature*, 2002, **417**, 813–821.
5 W. Rongchapo, *Water Sci. Technol.*, 2015, **71**, 1347–1353.
6 H. S. Cerqueira, P. C. Mihindou-Koumba, P. Magnoux and M. Guisnet, *Ind. Eng. Chem. Res.*, 2001, **40**, 1032–1041.
7 D. W. Breck, Crystallyne zeolite Y, *US Pat.*, US3130007, 1964.
8 E. C. Soule, N. Falls, *US Pat.*, 1959, 19–22.
9 R. Milton, Molecular sieve adosorbents, *US Pat.*, US2882243A, 1959.
10 X. P. Xiao, B. Q. Xiong, Q. S. Wang, G. L. Xie, L. J. Peng and G. X. Huang, *Rare Met.*, 2013, **32**, 144–149.
11 C. H. Rüscher, N. Salman, J. C. Buhl and W. Lutz, *Microporous Mesoporous Mater.*, 2006, **92**, 309–311.
12 K. M. Muirhead and N. P. Botting, *ARKIVOC*, 2002, **2002**, 37–45.
13 A. M. Yusof, N. A. Nizam and N. A. A. Rashid, *J. Porous Mater.*, 2010, **17**, 39–47.
14 T. Frising and P. Leflaive, *Microporous Mesoporous Mater.*, 2008, **114**, 27–63.
15 S. S. Bukhari, J. Behin, H. Kazemian and S. Rohani, *Can. J. Chem. Eng.*, 2015, **93**, 1081–1090.
16 L. Weber, K. Illgen and M. Almstetter, *Synlett*, 1999, 366–374.
17 R. W. Armstrong, A. P. Combs, P. A. Tempest, S. D. Brown and T. A. Keating, *Acc. Chem. Res.*, 1996, **29**, 123–131.
18 K. Ahmed, B. Dubey, S. Nadeem, B. Shrivastava and K. Ahmed, *Der Pharma Chem.*, 2015, **7**, 256–271.
19 A. Dömling and I. Ugi, *Angew. Chem., Int. Ed.*, 2000, **39**, 3168–3210.
20 P. S. G. Nunes, H. D. A. Vidal and A. G. O. Correâ, *Org. Biomol. Chem.*, 2020, **18**, 7751–7773.
21 M. C. Bagley, J. W. Dale and J. Bower, *Chem. Commun.*, 2002, **2**, 1682–1683.
22 S. L. Cui, X. F. Lin and Y. G. Wang, *J. Org. Chem.*, 2005, **70**, 2866–2869.
23 Y. Huang, F. Yang and C. Zhu, *J. Am. Chem. Soc.*, 2005, 16386–16387.
24 N. M. Evdokimov, I. V. Magedov, A. S. Kireev and A. Kornienko, *Org. Lett.*, 2006, **8**, 899–902.
25 K. Ahmed, B. Dubey, S. Nadeem and B. Shrivastava, *Chin. Chem. Lett.*, 2016, **27**, 721–725.
26 M. M. Heravi, H. Alinejhad, K. Bakhtiari, Z. Daroogheha, F. F. Bamoharram, F. Derikvand and B. Alimadadi, *ChemInform*, 2010, **41**, 52–161.
27 A. Agarwal, P. P. Pearson, E. W. Taylor, H. B. Li, T. Dahlgren, M. Herslöf, Y. Yang, G. Lambert, D. L. Nelson, J. W. Regan and A. R. Martin, *J. Med. Chem.*, 1993, **36**, 4006–4014.
28 S. M. Sondhi, J. Singh, R. Rani, P. P. Gupta, S. K. Agrawal and A. K. Saxena, *Eur. J. Med. Chem.*, 2010, **45**, 555–563.

29 Q. Xiao, L. Wang, S. Supekar, T. Shen, H. Liu, F. Ye, J. Huang, H. Fan, Z. Wei and C. Zhang, *Nat. Commun.*, 2020, **11**, 5430–5440.
30 V. Wankhade, A. R. Malu and S. P. Pawar, *Biol. Med.*, 2009, **1**, 122–126.
31 R. S. Upadhayaya, P. D. Shinde, S. A. Kadam, A. N. Bawane, A. Y. Sayyed, R. A. Kardile, P. N. Gitay, S. V. Lahore, S. S. Dixit, A. Földesi and J. Chattopadhyaya, *Eur. J. Med. Chem.*, 2011, **46**, 1306–1324.
32 Y. L. Chen, H. M. Hung, C. M. Lu, K. C. Li and C. C. Tzeng, *Bioorg. Med. Chem.*, 2004, **12**, 6539–6546.
33 E. L. Flannery, A. K. Chatterjee and E. A. Winzeler, *Nat. Rev. Microbiol.*, 2013, **11**, 849–862.
34 T. Sunami, K. Nishio, F. Kanzawa, K. Fukuoka, S. Kudoh, J. Yoshikawa and N. Saijo, *Cancer Chemother. Pharmacol.*, 1999, **43**, 394–401.
35 G. J. Atwell, G. W. Rewcastle, B. C. Baguley and W. A. Denny, *J. Med. Chem.*, 1987, **30**, 664–669.
36 J. A. Spicer, S. A. Gamage, G. J. Atwell, G. J. Finlay, B. C. Baguley and W. A. Denny, *J. Med. Chem.*, 1997, **40**, 1919–1929.
37 G. Kohlhagen, K. D. Paull, M. Cushman, P. Nagafuji and Y. Pommier, *Mol. Pharmacol.*, 1998, **54**, 50–58.
38 F. Shirini, S. S. Beigbaghlou, S. V. Atghia and S. A. R. Mousazadeh, *Dyes Pigm.*, 2013, **97**, 19–25.
39 S. M. Drechsel, R. C. K. Kaminski, S. Nakagaki and F. Wypych, *J. Colloid Interface Sci.*, 2004, **277**, 138–145.
40 S. A. Yashnik, V. F. Anufrienko, V. I. Zaikovskii, V. A. Rogov, S. P. Ruzankin and Z. R. Ismagilov, *Stud. Surf. Sci. Catal.*, 2008, **174**, 177–180.
41 G. Moretti, *Catal. Lett.*, 1994, **28**, 143–152.
42 G. Moretti, C. Dossi, A. Fusi, S. Recchia and R. Psaro, *Appl. Catal., B*, 1999, **20**, 67–73.
43 C. Lamberti, S. Bordiga, M. Salvalaggio, G. Spoto, A. Zecchina, F. Geobaldo, G. Vlaic and M. Bellatreccia, *J. Phys. Chem. B*, 1997, **101**, 344–360.
44 G. Turnes Palomino, P. Fisicaro, S. Bordiga, A. Zecchina, E. Giamello and C. Lamberti, *J. Phys. Chem. B*, 2000, **104**, 4064–4073.
45 Y. Kuroda, R. Kumashiro, T. Yoshimoto and M. Nagao, *Phys. Chem. Chem. Phys.*, 1999, **1**, 649–656.
46 Y. Kuroda, T. Mori, Y. Yoshikawa, S. Kittaka, R. Kumashiro and M. Nagao, *Phys. Chem. Chem. Phys.*, 1999, **1**, 3807–3816.
47 S. J. Tu, B. Jiang, R. H. Jia, J. Y. Zhang, Y. Zhang, C. S. Yao and F. Shi, *Org. Biomol. Chem.*, 2006, **4**, 3664–3668.
48 X. S. Wang, M. M. Zhang, H. Jiang, C. S. Yao and S. J. Tu, *Tetrahedron*, 2007, **63**, 4439–4449.
49 M. M. Heravi, H. Alinejhad, K. Bakhtiari, Z. Daroogheha, F. F. Bamoharram, F. Derikvand and B. Alimadadi, *Synth. Commun.*, 2010, **40**, 2191–2200.
50 Q. H. To, Y. R. Lee and S. H. Kim, *Bull. Korean Chem. Soc.*, 2012, **33**, 1170–1176.
51 S. Abdolmohammadi, *Chin. Chem. Lett.*, 2013, **24**, 318–320.
52 P. N. Sudhan, M. Ghashang and S. S. Mansoor, *Iran. J. Sci. Technol. Trans. A-Science*, 2018, **42**, 1895–1904.
53 M. M. Rahman, N. Hasnida and W. B. Wan Nik, *J. Sci. Res.*, 2009, **1**, 285–291.
54 N. S. Gould and B. Xu, *J. Catal.*, 2018, **358**, 80–88.
55 C. Boruban and E. Nalbant Esenturk, *J. Mater. Res.*, 2017, **32**, 3669–3678.
56 S. Ye, J. Sun, X. Yi, Y. Wang and Q. Zhang, *Sci. Rep.*, 2017, **7**, 1–9.
57 K. Phiwdang, S. Suphankij, W. Mekprasart and W. Pecharapa, *Energy Procedia*, 2013, **34**, 740–745.
58 A. K. Sasmal, S. Dutta and T. Pal, *Dalton Trans.*, 2016, **45**, 3139–3150.
59 A. Niftaliyeva, F. Güleç and A. Karaduman, *Res. Chem. Intermed.*, 2020, **46**, 2403–2416.
60 E. Tey, M. Hashim and I. Ismail, *Mater. Sci. Forum*, 2016, **846**, 471–478.
61 G. V. Sagar, P. V. R. Rao, C. S. Srikanth and K. V. R. Chary, *J. Phys. Chem. B*, 2006, **110**, 13881–13888.
62 J. J. F. Saceda, R. L. De Leon, K. Rintramee, S. Prayoonpokarach and J. Wittayakun, *Quim. Nova*, 2011, **34**, 1394–1397.
63 S. K. Kim, K. H. Kim and S. K. Ihm, *Chemosphere*, 2007, **68**, 287–292.
64 P. Karandikar, M. Agashe, K. Vijayamohanan and A. J. Chandwadkar, *Appl. Catal., A*, 2004, **257**, 133–143.
65 R. K. Nesbet, *J. Chem. Phys.*, 1964, **40**, 3619–3633.
66 Y. C. Zhang, J. Y. Tang, G. L. Wang, M. Zhang and X. Y. Hu, *J. Cryst. Growth*, 2006, **294**, 278–282.
67 M. Parhizkar, N. Kumar, P. K. Nayak, S. Singh, S. S. Talwar, S. S. Major and R. S. Srinivasa, *Colloids Surf., A*, 2005, **257–258**, 445–449.
68 W. T. Yao, S. H. Yu, Y. Zhou, J. Jiang, Q. S. Wu, L. Zhang and J. Jiang, *J. Phys. Chem. B*, 2005, **109**, 14011–14016.
69 B. K. Singh, Y. Kim, S. Kwon and K. Na, *Catalysts*, 2019, **9**, 1–12.
70 A. Seidel, J. Loosj and B. Boddenberg, *J. Mater. Chem.*, 1999, **9**, 2495–2498.
71 A. A. Alswata, M. Bin Ahmad, N. M. Al-Hada, H. M. Kamari, M. Z. Bin Hussein and N. A. Ibrahim, *Results Phys.*, 2017, **7**, 723–731.
72 T. Cui, Z. Liu, X. Zheng, Z. Liu, Y. Li, W. Li, B. Wang, K. Guo and J. Han, *Stud. Surf. Sci. Catal.*, 2008, **174**, 177–180.